

Strain Controlled Low Cycle Fatigue Behaviour of Type 304 SS Base, Type 308 SS Weld and 304/308 SS Weldments

K. Bhanu Sankara Rao*, M. Valsan*, S.L. Mannan*

1. INTRODUCTION

The emergence of liquid metal fast breeder reactor (LMFBR) technology made it necessary to use austenitic stainless steels at elevated temperatures where the mechanical properties are significantly influenced by time and cycle dependent phenomenon such as creep and low cycle fatigue (LCF). Many structural components in LMFBR's experience cyclic plasticity as a result of start-up and shut-down procedures. Cyclic deformation and fracture behaviour of the components are influenced by the presence of welds.

Often, fracture in fabricated engineering structures initiates at welded joints. The welding process produces local microstructural changes that are seldom considered in the operational design analysis. The metallurgical condition of the material is changed; local residual stresses of magnitude well beyond the component design stress may be introduced and frequently the defects are produced during the welding process which go sometimes undetected. These defects, together with unfavorable design geometries provide further stress concentrations, usually in regions of metallurgically susceptible microstructures. These combined effects on low cycle fatigue behaviour are often overlooked by the designer, fabricator and user of the component.

In the present study, the comparative evaluation of LCF lives and cyclic stress-strain properties of type 304 stainless steel base metal, 308 stainless steel weld metal and 304/308 weldments prepared by the manual metal arc welding process has been carried out at 823 and 923K. A detailed examination of the microstructural changes and the crack initiation and propagation behaviour has been conducted with a view to understanding the features which may influence the fatigue lives of defect free all weld metal and composite specimens. The influence of a specific heat treatment (1173K/3h) on LCF lives and cyclic

stress response behaviour of type 304/308 weldments has also been explored at 823K.

2. EXPERIMENTAL PROCEDURES

2.1 Welding Procedure and Specimen Details

The base material chosen for the investigations conducted here was a nuclear grade stainless steel conforming to AISI Type 304 specification. Chemical composition in weight % is given in Table 1. This material differs from the normal variety in that it has closely controlled composition, lower residual element concentration and inclusion content.

600 X 150 X 25 mm thick sections cut from the mill annealed plate were joined along the 600 mm length by manual metal arc welding process using 3.15 mm dia E 308-15 basic coated electrodes. Welding electrodes were dried for 1h at 473K before the commencement of welding. During welding the voltage and current were maintained at 25V and 150A approximately. Two types of weld joints were used in this work. All weld specimens were taken from the weld pads prepared with a 20 deg. included angle V-groove joint geometry with a 25 mm root gap and a backing strip. Typically, filling of this joint required 25 weld passes. Weldment specimens, comprising of base metal, weld metal and heat affected zone, were machined from the weld pads fabricated with a double-V configuration with an included angle of 70 deg. and a root face of 2 mm and a root gap of 3.15 mm. Approximately, 15 passes were used to complete double-V joint and the final weld has on "hour glass" shape and is almost symmetrical about the mid plane of the plate (Fig. 1). An interpass temperature of 423K was maintained during welding of both single-V and double-V weld joints. Subsequent to welding, the weld pads were examined, non-destructively by X-radiography to ensure their soundness, followed by delta-ferrite measurement using a commercial magnegaug. The ferrite contents reported are the statistical averages of at least 50 readings. An average analysis of the chemical composition of the type 308 stainless steel weld metal is given in Table 1.

This paper was presented in the National Welding Seminar, December 27-29, 1989, New Delhi. The authors are with Indira Gandhi Centre for Atomic Research, Kalpakkam.

Table 1. Chemical Composition of Base and Weld Materials (in Weight %)

	C	Si	Mn	P	S	Cr	Ni	Fe
AISI 304 SS (Base)	0.042	0.38	1.65	0.024	0.003	18.2	9.2	Balance
AISI 308 SS (Weld)	0.028	0.48	1.4	0.050	0.004	20.1	9.9	Balance

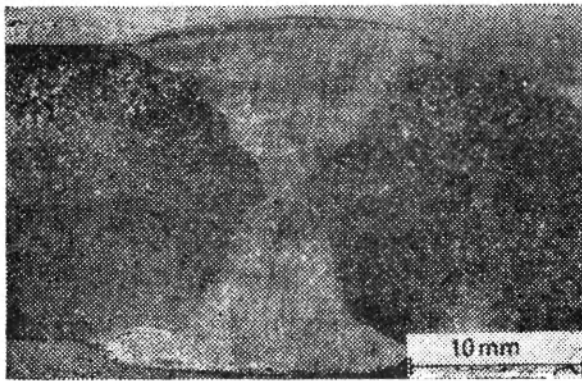
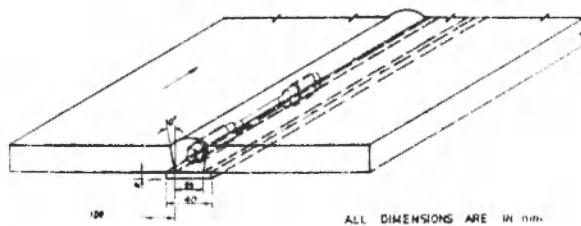
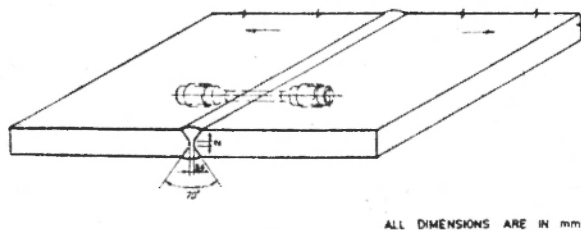


Fig. 1. "Hour Glass" shape of double-vee weldment



(a)



(b)

Fig. 2. (a) Allweldmetal test specimen
(b) LCF test specimen

50 mm gauge length and 10 mm dia axial cylindrical ridge LC specimens were machined from essentially the central sections of defect free single-V and double-V weld pads as per the lay out described in Fig. 2. Tensile test specimens were taken from the central sections of single-V joints such that the uniform gauge lengths of tensile specimens and LC specimens contain the similar amounts and morphology of delta-ferrite.

2.2 Low Cycle Fatigue and Tensile Testing

Fully reversed total axial strain controlled LCF tests were conducted at 823 and 923 K in air on base, all weld and weldment specimens, in an Instron 1343 Servo hydraulic system equipped with radiant heating facility. A constant frequency of 0.1 Hz was employed for the tests conducted over strain complitudes in the range of ± 0.25 to $\pm 0.80\%$. Temperature along the gauge part of a specimen was controlled to better than ± 2 K, and was monitored by a thermocouple placed in contact with the specimen. The total strain control mode of the testing was achieved by closed-loop control combination of a triangular wave input signal from the function generator and the averaged signal from the LVDT's of the LCF specimen. Stress strain hysteresis loops were recorded continuously to determine the cycle dependent changes in stress and plastic strain amplitudes.

Tensile tests were carried out on base and all weld metal in a floor model Instron 1195 universal testing machine equipped with three zone resistance furnace. Tests were performed in air over a temperature range 300-1023K at a nominal strain rate of $3 \times 10^{-3} \text{ s}^{-1}$.

2.3 Metallography

The polished samples were etched and examined using a Reichert MeF₂ optical microscope equipped with a camera. Several different etchants were utilized. For studying the morphology of delta-

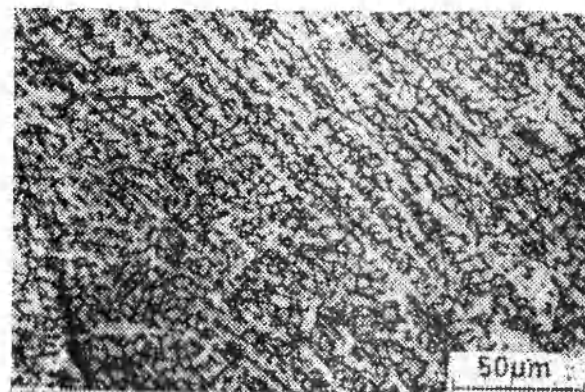
ferrite, the as deposited weld samples were etched in the boiling Murakami reagent (10 gm KOH, 10 gm $K_3 [Fe(CN)_6]$ and 100 ml water, for 3 minutes. The general microstructure of base and weldments was revealed after etching electrolytically in a solution containing 70% HNO_3 . LCF tested samples were sectioned parallel to the stress loading direction, polished, etched and examined under optical microscope to obtain the information on crack initiation and propagation modes and microstructural changes that occur during fatigue deformation. Tested samples of all weld and weldments were etched in a modified Murakami's reagent (30 gm KOH, 30 gm $K_3 [Fe(CN)_6]$ and 150 ml water) at 363 K for 15 seconds. This treatment caused sigma phase to be brownish red, ferrite to be dark gray, austenite to be light gray and carbides to be black. Fractography of the LCF tested specimens was carried out using a Philips PSEM 501 scanning electron microscope (SEM). Transmission electron microscopy [TEM] studies were carried out on LCF tested base material samples using Philips EM 400 Microscope.

3. RESULTS

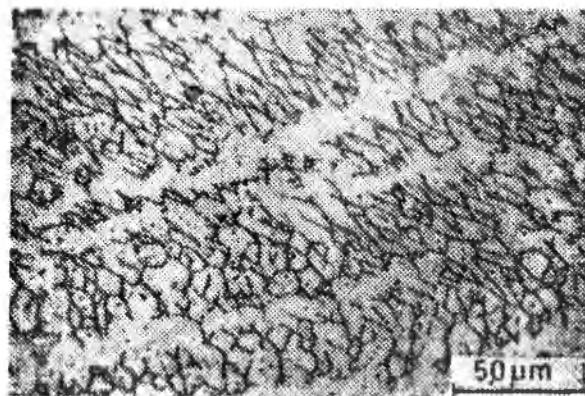
3.1 Microstructure Prior to LCF Testing

The average intercept grain size of the base material was 75µm and the microstructure was free from inclusions and undissolved carbides. The microstructures of the as deposited weld metal, made up of successively overlaid weld beads, were typical of type 308 stainless steel weld metal and was composed of long columnar grains and 9-12FN of delta-ferrite distributed in the austenite matrix.

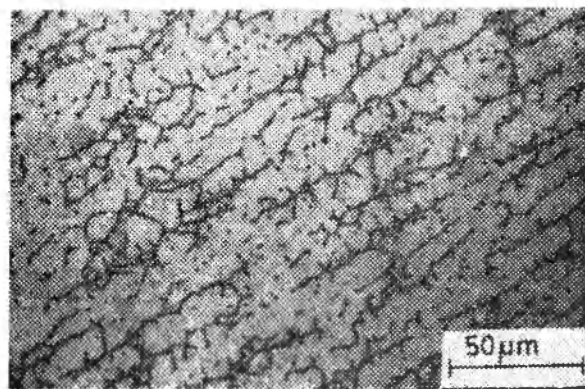
The amount, distribution and morphology of the as welded delta-ferrite varied from pass to pass but remained unchanged within a given pass. Typical morphologies of delta-ferrite seen in the multipass welds of single-V joint are depicted in Fig. 3. Fig. 3a describes the skeletal morphology observed in the top pass whereas Fig. 3b characterizes the lacy delta-ferrite seen in a few passes just below the top pass. The vermicular morphology shown in Fig. 3c represents the actual delta-ferrite structure of the gauge portions of LCF and tensile specimens. The ferrite content varied with its morphology (i.e.) position in the weld. The average delta-ferrite contents of the single-V weld in skeletal, lacy and vermicular morphology regions has been estimated as 12, 11.5 and 9.0 FN respectively. It can be seen that the delta-ferrite dendrites in lacy and vermicular morphology regions have contained finely distributed $M_{23}C_6$ carbides. Fig. 4 describes the representative microstructure in the gauge portion of LCF specimens



(a) The skeletal morphology of top pass



(b) The lacy delta-ferrite below the top pass



(c) The actual delta-ferrite in the gauge portion

Fig. 3. Typical morphologies of delta-ferrite in single-vee weldment

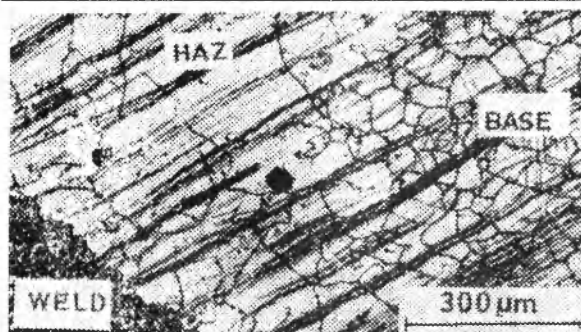
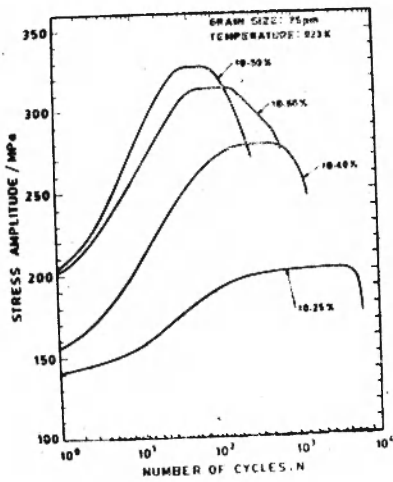
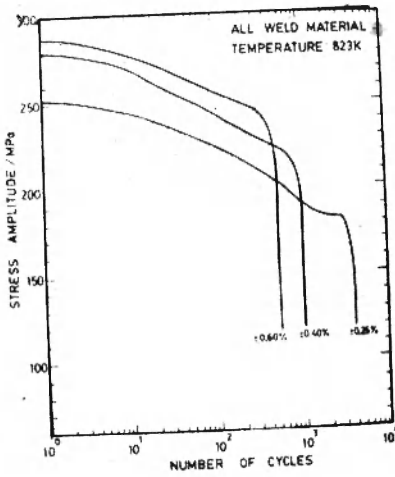


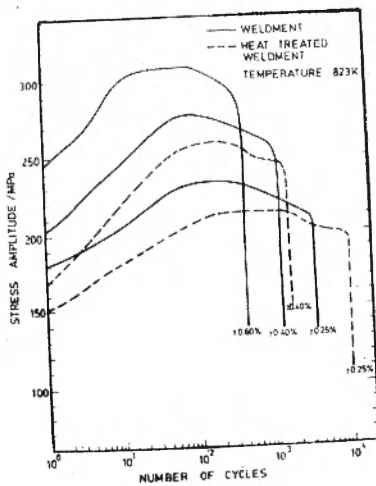
Fig. 4. The microstructure of gauge portion, double-V weldment



(a)

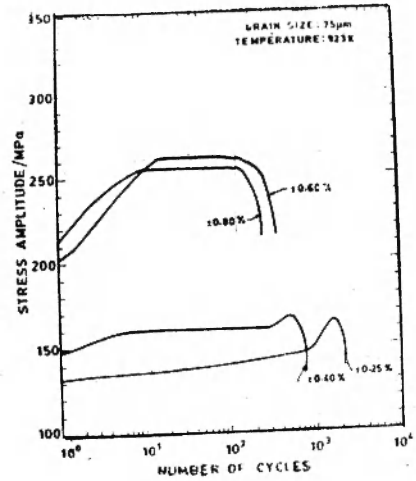


(b)

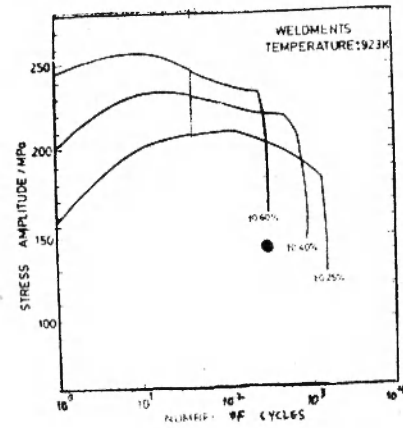


(c)

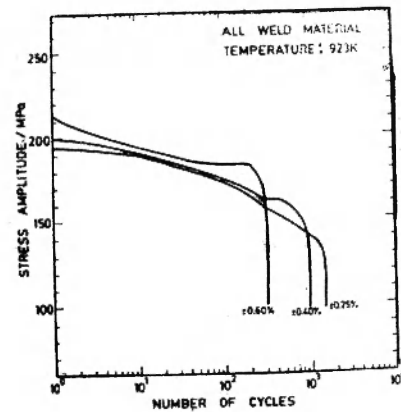
- (a) The base material
- (b) Allweld metal
- (c) The Weldment



(a)



(b)



(c)

- (a) The base material
- (b) Allweld metal
- (c) The Weldment

Fig. 5. The cyclic stress response curves at 823K

Fig. 6. The cyclic stress response curves at 923K

made out of double-V joint weldments. The coarse grained region adjoining to the weld metal depicts the HAZ, and its width is about approximately 1000 μm in size. The average delta-ferrite content of the weld metal in the composite LCF specimens was 9.0 FN.

3.2 Tensile Properties

Results of tension tests conducted on base and all weld metal as a function of temperature are given in Table 2. Base material exhibited higher ultimate tensile strength [UTS], and ductility (as measured by total elongation) compared to the weld metal at all the temperatures in the range 300-1023K. However, the weld material was found to have higher yield strength than the base material at all the temperatures. The yield and ultimate tensile strengths decreased gradually with increasing temperature in both the base and weld materials.

Table 2. Tensile properties of Base and All Weld Material at $\dot{\epsilon}=3 \times 10^{-3}\text{s}^{-1}$

TEST TEMP.	Y.S. (MPa)	U.T.S (MPa)	U.E. (%)	T.E. (%)
All Weld Material				
300 K	378	543	38	47
623 K	290	399	23	31
723 K	289	388	23	28
823 K	288	358	17	24
923 K	233	283	11	17
1023 K	176	198	10	36
Base Material				
300 K	296	615	53	65
623 K	159	449	36	42
723 K	155	430	35	41
823 K	154	412	34	40
923 K	142	349	33	43
1023 K	111	253	26	47

3.3 Low Cycle Fatigue

3.3.1 Stress Response Curves

The cyclic stress response curves obtained by plotting the peak tensile stress amplitude versus number of cycles in a total strain controlled fatigue test illustrate the path by which the material arrives at its final cyclic flow stress level. The cyclic stress response curves obtained at 823 and 923K for the base, all weld and weldments are shown in Figs.5 and 6 respectively. At 823K, at all strain amplitudes, the base material (Fig.5a) has undergone very rapid strain hardening to a maximum cyclic stress in the early stages of fatigue test; followed by an extended stage of saturation stress response,

which persisted, until the crack nucleation and growth impaired the load carrying capacity of the specimen, which was indicated by the rapid fall of the stress towards the end of test. The proportion life spent in the stable state decreased with increasing strain amplitude. At 923K, base material displayed pronounced secondary hardening peak at low strain amplitudes as depicted in Fig. 6a, however, at high strain amplitudes the stress response was similar to that observed at 823K.

All weld metal exhibited cyclic softening to failure from the onset of cyclic deformation both at 823K (Fig.5b) and 923K (Fig. 6b) displayed cyclic hardening initially, followed by gradual softening before the onset of rapid drop in stress towards the end. Generally the heat treated weldments showed a short period of cyclic hardening followed by gradual softening to a saturation stress value (Fig. 5c). The pronounced saturation stage could not be seen in the as-welded condition of weldments.

3.3.2 Cyclic Stress-Strain Curves (CSSC)

From the cyclic stress response curves the cyclic stress-strain curves for base and weld metal were deduced to facilitate the comparison of monotonic and half-life CSSC of the base and all weld metal at

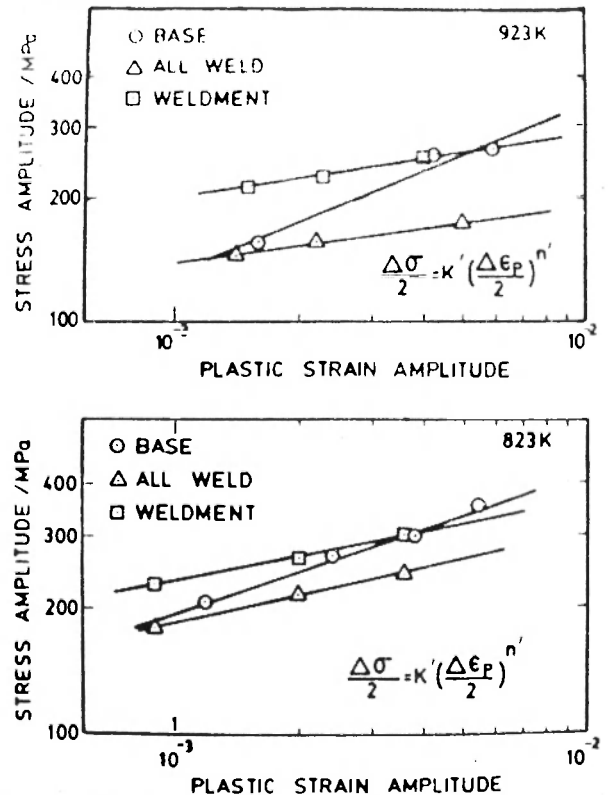


Fig. 7. Representation of the Power Law at 823K & 923K. Values of K' and n' presented in Table 3.

Table 3. Summary of the constants in Cyclic Stress-Strain Relationship, Basquin and Coffin-Manson Relationships

TEMP.	MATERIAL CONDITION	n'	K ¹	c	ε' _f	b	σ' _f	2N _f
823 K	BASE	0.344	2230	-0.502	0.122	-0.207	1550	7.6x10 ³
	ALL WELD	0.218	900	-0.430	0.338	-0.158	1612	2.2x10 ³
	WELDMENT	0.204	1000	-0.681	0.395	-0.146	899	2.5x10 ³
923 K	BASE	0.396	2210	-0.560	0.190	-0.368	2812	9.0x10 ⁴
	ALL WELD	0.136	365	-0.579	0.230	-0.284	1731	5.8x10 ³
	WELDMENT	0.158	605	-0.642	0.273	-0.169	1110	1.9x10 ³

823K and 923K respectively. From the relative positioning of monotonic and CSSC, it is possible to predict qualitatively whether cyclic hardening or softening will occur. At both the temperatures CSSC of weld metal is lower than the monotonic curve indicating the generally observed tendency for cyclic softening in the full range of strain amplitudes examined. Similarly, the exhibited tendency of base material for cyclic hardening is indicated by CSSC having higher values than monotonic ones at all the strain amplitudes investigated. The half-life cyclic stress-strain curves of the base, all weld and weldments, could be represented by a power law of the form $\Delta\sigma/2 = K'(\Delta\varepsilon_p/2)^{n'}$ where K' and n' cyclic strain hardening exponent respectively. The data following the above equation at 823 and 923K on log-log co-ordinates is shown in Fig. 7. A tabulation of K' and n' values for three material conditions is presented in Table 3.

3.3.3 Fatigue Life

Results of the strain controlled fatigue tests at 823 and 923K are shown in Tables 4 and 5 respectively. Cyclic life (N_f) was defined to be the number of the cycles corresponding to a 20 % reduction in the tensile stress; the tensile stress measured at about half of the estimated cyclic life as 100 percent. This was necessary since, in some instances, specimen failure (separation into two halves) only occurred after the tensile stress had decreased to a very low value. Hence, defining failure in this manner provided a uniform definition from specimen to specimen which in most instances was within 5% of separation value (N_{sep})^{7,8}. It has also been suggested that such a definition for failure life avoids possible damage to the expensive extensometry and grips which might occur on specimen rupture and prevents the hammer damage to the fracture surfaces which can obliterate valuable fractographic information.

The values of total strain amplitude ($\Delta\varepsilon_f/2$), plastic strain amplitude ($\Delta\varepsilon_p/2$) and saturation stress amplitude ($\Delta\sigma/2$) sat, measured from half-life (N_f/2) stress-strain hysteresis loops of various tests are given in Tables 4 and 5.

Figs. 8 and 9 show the fatigue life results as double logarithmic plots between $\Delta\varepsilon_f/2 - 2N_f$ (number of reversals to failure) and $\Delta\varepsilon_p/2 - 2N_f$ at 823 and 923K respectively. The fatigue lives of the base, all weld and weldment at both the temperatures have been found to follow the strain-life relationship derived by Raske and Morrow⁹ and Landgraf et.al.¹⁶ based on the relationships proposed by Basquin¹¹ and Coffin-Manson^{12,13}. The strain-life relationship is given by $\Delta\varepsilon_f/2 = \Delta\varepsilon_p/2 + \Delta\varepsilon_p/2 = \sigma_f/E(2N_f)^b + \varepsilon_f(2N_f)^c$

where σ_f = fatigue strength co-efficient,
 b = fatigue strength exponent,
 ε_f = fatigue ductility co-efficient,
 c = fatigue ductility exponent,
 and E = Elastic Modulus

Values of the constants and co-efficients for the above equation as established by least square analysis are summarized in Table 3 for the temperatures and material conditions investigated.

Transition fatigue life (2N_f), was obtained as the intersection point between $\Delta\varepsilon_f/2 - 2N_f$ and $\Delta\varepsilon_p/2 - 2N_f$ curves as depicted in Fig. 10 for the data at 923 K. 2N_f values for the different conditions are given in Table 3.

3.3.4 Evolution of Microstructure During Fatigue Deformation

Metallographic examination carried out on the LCF tested specimens indicated that the vermicular delta-ferrite present in as-welded condition has undergone decomposition (Fig. 11). Extensive precipitation of M₂₃C₆ carbides and sigma phase was observed preferentially on the boundaries between the austenite and ferrite phases. The measured FN

Table 4. Low Cycle Fatigue Properties of Base Metal, All Weld Metal and Weldments at 823K

Material Condition	Sample Code	$\Delta \epsilon_t / 2$ (%)	$\Delta \epsilon_s / 2$ (%)	$\Delta \epsilon_o / 2$ (%)	$\Delta \sigma / 2$ (MPa) (First)	$\Delta \sigma / 2$ (MPa) (Sat)	Cycles	
							N_{sep}	N_f
BASE	108	0.25	0.12	0.13	140	208	6280	6211
	109	0.40	0.24	0.16	159	271	1475	1290
	110	0.60	0.38	0.22	200	300	670	630
	111	0.80	0.54	0.26	205	316	295	295
ALL WELD	W04	0.25	0.09	0.16	252	181	3900	3760
	W03	0.25	0.09	0.16	254	188	4360	4130
	W01	0.40	0.20	0.20	278	220	1120	1015
	W02	0.60	0.36	0.24	288	245	560	528
WELDMENTS	J04	0.25	0.09	0.16	181	232	3560	3360
	J01	0.40	0.21	0.18	197	277	1250	1140
	J02	0.60	0.37	0.23	245	306	435	392
STRESS RELIEVED JOINTS	SRJ01	0.25	0.11	0.14	150	210	10010	9890
	SRJ02	0.39	0.22	0.17	169	252	15055	1512

Table 5. Low Cycle Fatigue Properties of Base Metal, All Weld Metal and Weldments at 923K

Material Condition	Sample Code	$\Delta \epsilon_t / 2$ (%)	$\Delta \epsilon_s / 2$ (%)	$\Delta \epsilon_o / 2$ (%)	$\Delta \sigma / 2$ (MPa) (First)	$\Delta \sigma / 2$ (MPa) (Sat)	Cycles	
							N_{sep}	N_f
BASE	112	0.25	0.16	0.09	132	155	2285	2200
	113	0.40	0.30	0.10	148	162	710	650
	114	0.60	0.42	0.19	202	258	370	345
	115	0.80	0.59	0.21	214	260	250	220
ALL WELD	W05	0.60	0.41	0.18	214	175	355	322
	W06	0.25	0.13	0.12	194	147	1770	1615
	W07	0.40	0.22	0.18	201	159	1015	945
WELDMENTS	J05	0.40	0.23	0.17	201	223	820	778
	J06	0.60	0.42	0.18	245	250	330	280
	J07	0.25	0.15	0.10	158	212	1540	1375

decreased in LCF tested samples. The decrease in measured FN resulted primarily from transformation of ferrite in the structure to sigma phase (non-magnetic). The extent of delta-ferrite transformed the structure depended upon the material condition, temperature and strain amplitude employed in LCF testing and the number of cycles seen by the samples. In general, the fraction of delta-ferrite transformed showed an increase with increasing temperature, and increasing number of cycles to

failure (N_{max}). The transformation of delta-ferrite in weldments was found to be more than in weld metal at identical testing conditions.

In base material, during deformation at 923K, dislocations, dislocation tangles and planar slip bands acted as the preferential sites for nucleation of $M_{23}C_6$ particles. At 823K at all amplitudes, base material displayed homogeneously distributed dislocations and dislocation tangles. $M_{23}C_6$ precipitation was not disordered at 823K in base material.

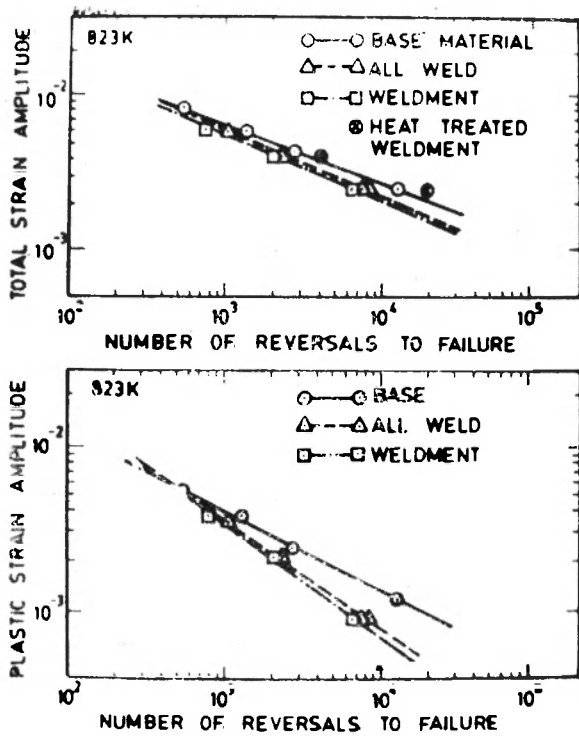


Fig. 8 Fatigue life results at 823K

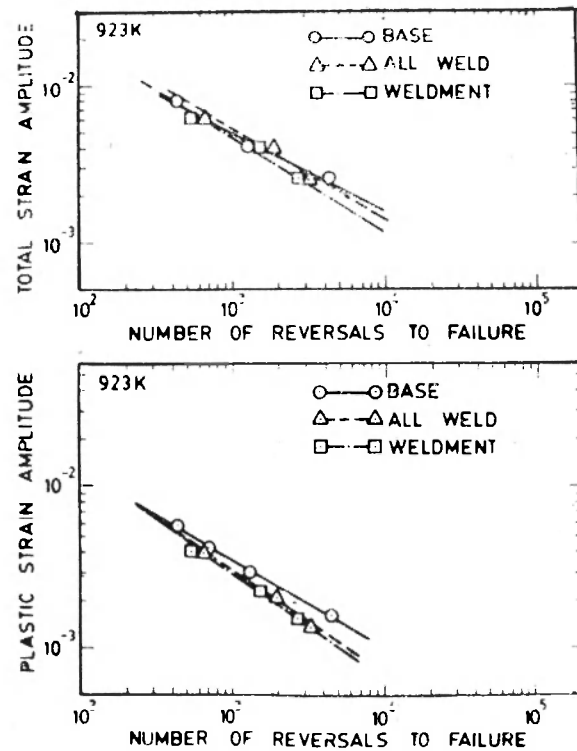


Fig. 9 Fatigue life results at 923K

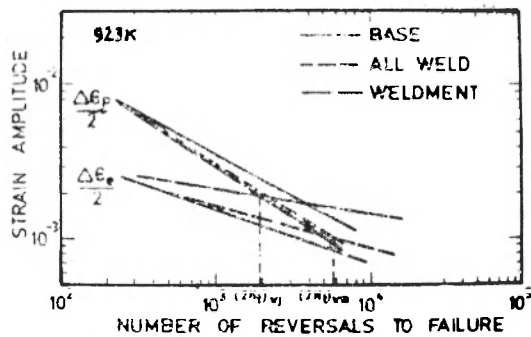


Fig. 10 Transition fatigue life ($2N_p$) results from data at 923K

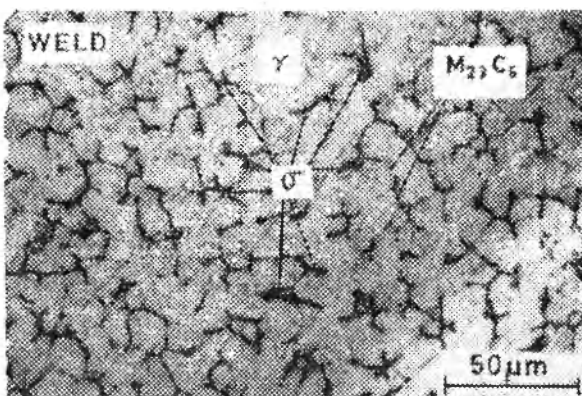
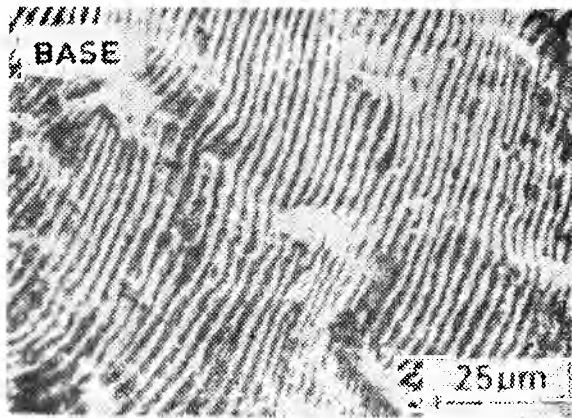


Fig. 11 Microphotograph of LCF tested specimen showing decomposition of vermiculite delta-ferrite in as welded condition

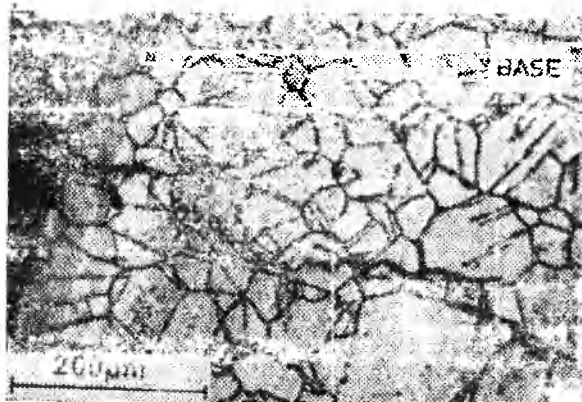
3.3.5 Fractographic and Metallographic Observations on LCF Tested Samples

In base material, at 823K, at all strain amplitudes, fatigue crack initiation took place along the persistent slip bands. Initial propagation of slip band cracks occurred along the slip planes which were oriented nearly at 45° to the applied stress axis, designated at stage-I¹⁴. Stage-I cracking continued to only one or two grain diameters into the specimen, before a transition to transgranular state-II cracking occurred. Stage-II transgranular cracking was characterized by the occurrence of well defined ductile striations on fracture surface¹⁷. Fig. 12a illustrates the typical fractograph depicting the ductile striations on the fracture surface of base metal tested at 823K with $\Delta\epsilon/2 = \pm 0.40\%$. As at 823K, cracks in base metal at 923K also initiated and propagated transgranularly but oxidation assisted. Studies on macrocracks of the longitudinally sectioned specimens clearly illustrated the transgranular crack initiation and propagation in base material at 923K, (Fig. 12b).

In all weld metal, at both the temperatures, fatigue crack initiation was found to occur from the surface at the austenite-ferrite interfaces. Crack propagation was generally transgranular. Crack path diversion was occasionally noticed along the transformed delta-ferrite regions. Fatigue striations showed a



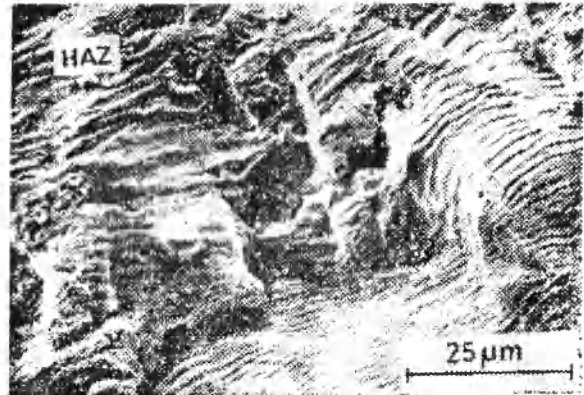
(a) Showing ductile striations on the fractured surface at 823K



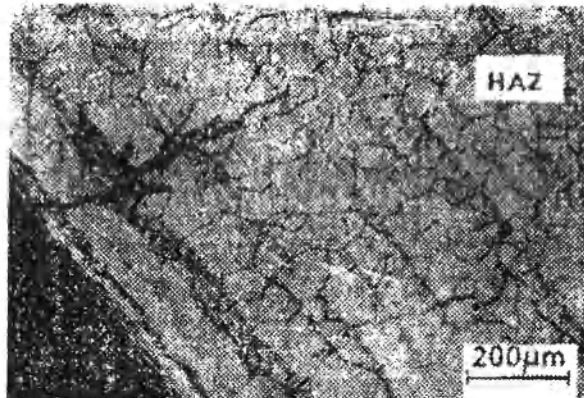
(b) Micrograph of longitudinally sectioned specimen, showing oxidation assisted, transgranular macrocrack, initiated and propagated



(a) LCF tested weldment specimen showing fatigue crack through HAZ



(b) Fracture surface at 823K



(c) Intergranular crack in HAZ at 923K



(d) Heat treatment of weldment at 1173K for 3 hrs. shifted the crack initiation to the weldmetal region

Fig. 12 Typical fractograph of the base material

brittle appearance and a striation cracking was predominant.

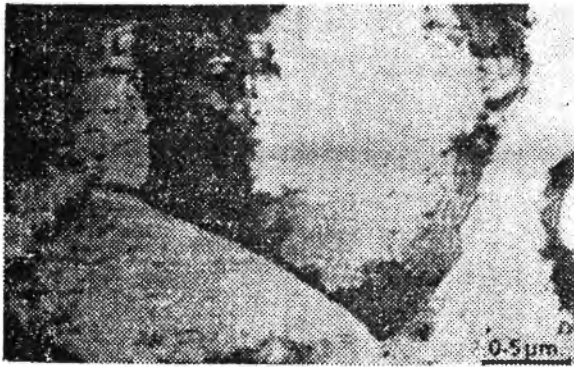
In the weldments at 823K, fatigue cracks initiated in PSB's in HAZ and propagated through HAZ in an orientation parallel to the fusion line (Fig. 13a). The fracture surface at 823K contained brittle striations (Fig. 13b). At 923K, crack initiation and initial propagation occurred intergranularly in HAZ (Fig. 13c) and seems to be oxidation assisted. At 923K, too, in later stages propagation remained transgranular. Heat treating the weldments at 1173K/3h, shifted the crack initiation and propagation to the weld regions (Fig. 13d).

Fig. 13

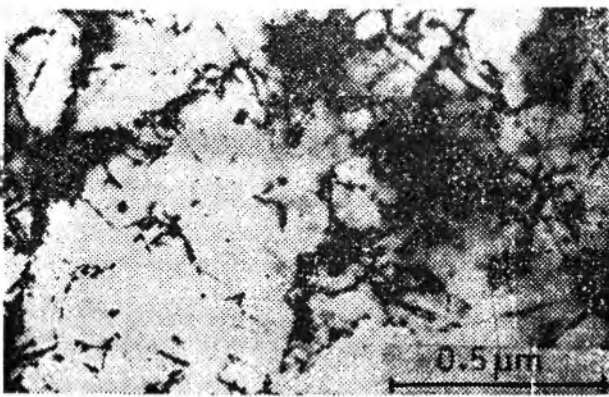
4. DISCUSSION

4.1 Cyclic Stress Response

Results clearly revealed that cyclic stress response is highly sensitive to the details of metallurgical condition of the material, temperature and strain amplitude employed during LCF testing. At 823K, base material exhibited pronounced cyclic hardening in the early stages (Fig.5a). In base material, cyclic



(a) Micrograph showing formation of cells and subgrains



(b) Micrograph showing carbide precipitation in matrix at dislocation and dislocation tangles

Fig. 14

stress response at 923K (Fig.6a) appears to be governed by two competitive processes, namely dynamic recovery (i.e.) the formation of cells and sub-grains (Fig. 14a) and precipitation of carbides in the matrix on the dislocations and dislocation tangles (Fig.14b). The dense tangles and precipitation stabilised dislocation substructures are expected to induce considerable cyclic hardening. In contrast, formation of cells and sub-grains due to dynamic recovery leads to cyclic softening. The secondary hardening at low strain amplitudes (Fig.6a) indicates that there is a significant contribution of $M_{23}C_6$ precipitation on dislocations to the matrix strengthening behaviour. A balance between dynamic recovery and strengthening due to intragranular carbide precipitation at high strain amplitudes leads to a saturation stage. In the absence of dynamic recovery and precipitation, the stable stress response stage at 823K (Fig.5a) could be attributed to the saturation in the development of dislocation density in the matrix.

All weld metal displayed pronounced softening to failure at all the strain amplitudes at 823K (Fig.5b)

and 923K (Fig.6b). In our study samples for LCF testing were taken from the central regions of weld pads. It has been shown by King et al.²⁶ in type 308 SS welds, the central regions of the weld metal contain very high dislocation densities than surface regions.

In contrast to the all weld metal, weldments comprising base, weld and HAZ showed cyclic hardening initially (Fig.5c and Fig.6c) like the base material (Fig.5a and Fig. 6a). It must be mentioned that the major part of the gauge length portion was made up of base material. Therefore, it is reasonable to expect that the initial cyclic deformation behaviour of the weldment would be similar to that of its major constituent. Two major differences existed between the base and weldment stress response. Weldments did not show the stable stress response period like base material, and the onset of stress drop occurred much earlier in weldment than in base at identical strain amplitudes at both the temperatures. This observation indicates that the microcrack initiation in weldment occurred sooner than in base material. Microcrack initiation occurs in weldment early because of the cracking at austenite-sigma interfaces.

4.2 Fatigue Life

The influence of the metallurgical state of the material on the LCF life is demonstrated in Tables 4 and 5 and in Figs. 8 and 9. In general, base material displayed better endurance than all weld metal and weldments in terms of total and plastic strain amplitudes at both 823 and 923K. Weldments showed inferior fatigue resistance of all while weld metal fatigue resistance was only marginally better than that of weldments. Reduced strain controlled fatigue resistance for weldments was not surprising considering the presence of coarse grain size in the HAZ (Fig.4) which could act as a metallurgical notch. At 823K, in base and weldments the crack initiation occurred in persistent slip bands which signifies the occurrence of planar slip. A number of investigators^{18,31-33} have reported the deleterious effects of coarse grain size in alloys deforming by planar slip. Since grain size governs the slip length, a coarse grain size can be expected to develop larger slip steps at the surface, which would render the formation of intrusions and extrusions more easy. Intrusions act as notches from which cracks originate. Therefore, it is reasonable to assume that the coarse grain size in HAZ might have shortened the crack initiation stage. Furthermore, in alloys deforming by planar slip, the improved crack propagation resistance has been noticed, with decreasing grain size^{34,35}, and

has been ascribed to the fact that the grain boundaries serve as the natural barriers to transgranular crack propagation³⁶, causing the crack front to be held back and necessitating the crack reinitiation even to occur in each new grain. Since at 823K in the weldments crack propagated transgranularly in the HAZ containing coarse grain size, it can be argued that crack propagation resistance in weldments is also reduced.

All weld metal showed inferior fatigue resistance compared to base metal at both 823 and 923K. This result is in close agreement with those obtained by Brinkman et al² on type 304 SS base and type 308 SS welds at 866 K. Fatigue life is generally governed by the ductility of the material at high strain amplitudes and by the strength of the material at low strain amplitudes. All the fatigue tests in the investigation were performed at reasonably high strain amplitudes. Fatigue damage in strain controlled fatigue testing results from the repeated plastic strains. The reduction in fatigue life of all weld material compared to base material is generally attributable to the reduced tensile ductility of weld material (Table 2); the fatigue life, particular for large strain amplitudes (which are mostly plastic, Table 4 and 5) would thus be reduced. This argument may also hold good to a certain extent to the weldments because, the type 304 SS base metal near the fusion line is stronger due to high dislocation density introduced by thermo-mechanical cycling during welding but less ductile than base metal unaffected by welding.

All the three conditions exhibited shorter fatigue lives as the temperature was increased from 823 to 923K, indicating that crack initiation or propagation, or both, took place more rapidly at high temperature. At high temperatures creep and/or environmental effects become increasingly important. Examination of the areas ahead of microcracks of the longitudinally sectioned specimens and also the regions beneath the fracture surface of the base, all weld and weldment samples tested at 923 K failed to reveal either intergranular wedge cracking or void formation which would suggest the dominance of creep damage in fracture process. This is not surprising because the creep damage in a fatigue cycle was shown to depend upon the wave shape employed³⁷. Balanced cycles with equal strain rates in tension and compression, similar to the ones employed in this study have not produced bulk intergranular creep damage whereas it has been shown that bulk intergranular creep damage results by unbalanced cycles comprised of slow tensile going ramp and fast compressive going ramp (slow-fast cycle) or tensile holds³⁸.³⁹ Besides, it

must be mentioned, the short period of time associated with each fatigue test at 923K is insufficient to cause any significant creep damage. However, increases in inelastic strain in a cycle with increase in temperature were observed in case of base, all weld and weldments (Tables 4 and 5) and would lead to reduction of life at elevated temperatures.

At 923 K, in base, all weld (Fig.12b) and weldments (Fig.13c), the crack initiation and propagation was oxidation assisted. Environmental damage under a balanced hysteresis loop and high temperature has been shown by several investigators to play a significant role in governing fatigue. A model has been proposed by McMahan and Coffin⁴⁰ to explain accelerated crack initiation and propagation to environmental interaction. In this model the degradation in life was attributed to film rupture due to cyclic plastic deformation were considered to rapidly oxidise and aid in accelerating crack initiation and propagation. At 923K, in all weld metal, surface cracks initiated at austenite-ferrite boundaries (Fig.13a). Earlier results of crack growth rate studies on stainless steel weld-and-base metal specimens indicated that the weld metal has significantly lower crack-growth rates than the base metal, particularly at 866K^{41,43}. This difference has been attributed to the fine delta-ferrite-austenite microstructure in the weld metal which, with its many phase boundaries is believed to offer a greater resistance to the extension of fatigue cracks than does the relatively coarser structure of the base metal. However, in this study, at 923K, extensive transformation of ferrite to sigma phase occurred at gamma/delta interfaces, providing a variety of inter-phase boundaries to serve as the fracture paths. Extensive sigma phase formation at prior gamma-delta interfaces might lower the ductility locally and hence initiate crack. In fact large number of microcracks were observed on the fracture surface, of the welds and weldments due to cracking at the austenite-sigma interfaces. The larger reduction in fatigue lives observed in all weld and weldments at 923K particularly at low strain amplitudes could be attributed to the extensive transformation of delta to sigma and associated microcracking at the austenite-sigma interfaces. Joining of these microcracks with main crack shortens the crack propagation stage and hence leads to the over all reduction in fatigue life. Heat treating (1173K/3h) the weldment prior to LCF testing improved fatigue resistance significantly (Fig.8). This results from the relaxation of residual stresses and the beneficial changes that occur in the microstructure of weld and heat affected zones (HAZ).

5. CONCLUSIONS

1. Type 304 SS base material exhibited better strain controlled fatigue resistance than either type 308 SS all weld material or 304/308 SS weldments at 823 and 923 K. Weldments comprising of base, weld and heat affected zone showed the lowest fatigue resistance at both 823 and 923 K.
2. The loss of fatigue lives was observed when the temperature was raised from 823 to 923K in all the three material conditions (i.e. base, all weld and weldment). It was concluded that under the test conditions employed at 923K, LCF life is not governed by creep damage mechanisms.
3. It was found that the reduction in LCF life with increasing temperature results from an increase in inelastic strain generated in a cycle and from the effects of oxidation assisted crack initiation and propagation in all three material conditions.
4. The plastic strain amplitude versus number of reversals of failure plots obeyed the Coffin-Manson relationship at both 823 and 923K in all the three material conditions.
5. Typically, the type 308 SS weld material exhibited continuous cyclic softening until failure at both 823 and 923K at all strain amplitudes. Base material showed rapid initial hardening followed by a well defined saturation stress stage at 823K. At 923K, in base material secondary hardening preceded the rapid stress drop associated with the macrocrack initiation and propagation. At both 823 and 923K, weldments initially hardened and then softened gradually prior to the rapid stress decrease.
6. Half-life cyclic stress-strain curves of all the three material conditions obeyed the relationship $\Delta\sigma/2=K'(\Delta\varepsilon_p/2)^n$ at both the temperatures. Base material showed higher cyclic strain hardening exponent n' , than all weld and composite material vermicular delta-ferrite present in the all weld and weldments transformed to carbides and sigma phase. Transformation of delta-ferrite was rapid in weldment than in all weld material at 923K at all strain amplitudes. The proportion of delta-ferrite transformed increased with increasing number of cycles to failure in both weld and composite specimens. Sigma phase was believed to cause embrittlement locally and lead to the formation of microcracks

at austenite-sigma interfaces, which shorten macrocrack propagation stage in all weld and weldment material.

7. Solution treatment (1173K/3h) of the weldment prior to LCF testing lead to a drastic increase in fatigue life. The solution treated weldment exhibited strong cyclic hardening tendency in the initial stages as found in base and untreated weldment.

6. ACKNOWLEDGEMENT

The authors would like to thank Dr. Placid Rodriguez, Head, Metallurgy and Materials Programme for his encouragement and many helpful discussions. The help rendered by Miss R. Sandhya at various stages of this investigation is sincerely appreciated. Acknowledgments are due to Shri R. Balakrishnan for typing the manuscript.

REFERENCES

1. R.G. Gilliland; The Behaviour of Welded Joints in Stainless and Alloy Steels at Elevated Temperatures', U.S. AEC Report ORNL-4781, Aug. 1982.
2. C.R. Brinkman, G.E. Korth and J.M. Beeston; "Comparison of the Strain Controlled Low Cycle Fatigue Behaviour of Stain-Type 304/308 Weld and Base Material". Proc. Intl. Conf. on Creep and Fatigue in Elevated Temperature Applications, Philadelphia, Sept. 1973 and Sheffield U.K. April 1974, Inst. Mech. Engrs. (1974), paper C218/73, pp.218.1-218.11.
3. ASME Boiler and Pressure Vessel Code, Code Case N-37(1986).
4. D.P. Edmonds, D.M. Vandergriff and R.J. Gray, 'Effect of Delta-Ferrite content on the Mechanical Properties of E308-16 Stainless Steel Weld Metal' in Properties of Steel Weldments for Elevated Temperature Pressure Containment Applications, MPC-9, (Ed.) G.V. Smith, ASME. (1978), pp.47-61.
5. J.C. Borland and R.N. Young, 'Some Aspects of Cracking in Welded Chromium-Nickel Austenitic Steels', British Welding Research Association, London, England, BWRA Report-B5/1/59, Aug. 1959.

6. M.O. Malone, *Welding Journal*, 46 (1967), 241s.
7. K. Bhanu Sankara Rao, M. Valsan, R. Sandhya, S.K. Ray, S.L. Mannan and P. Rodriguez; *Intl. J. Fatigue*, 7 (1985), 141.
8. C.R. Brinkman, J.P. Strizak and J.F. King, *ASTM STP.*, 648 (1978), 218.
9. D.T. Raske and J. Morrow, *ASTM STP.*, 465 (1969), 1.
10. R.W. Landgraf, J. Morrow and T. Endo, *J. Materials, JMLSA.*, 4 (1969), 176.
11. O.H. Basquin, *Proc. Amer. Soc. Test. Meter.*, 10 (1910), 625.
12. L.F. Coffin, Jr., *Trans. Amer. Soc. Mech. Engrs.* 76 (1954), 923.
13. S.S. Manson, "Behaviour of Materials under Conditions of Thermal Stress", *Nat. Adv. Comm. Aero.*, (1954), Technical Note-2933.
14. W.H. Kim and C. Laird, *Acta Metall.*, 26 (1978), 789.
15. C. Laird, 'Mechanism and Theories of Fatigue' - Paper Presented at the Materials Science Seminar, ASM, St. Louis, Missouri (1978).
16. J.T. Berling and T. Slot, *ASTM STP.*, 459 (1969), 3.
17. C.E. Jaske, N.D. Fray and D.A. Utah, "Applications of Materials for Pressure Vessels and Piping" ed. G.V. Smith, ASME, (1976), pp. 75-109.
18. K.Bhanu Sankara Rao, "Influence of Metallurgical Variables on Low Cycle Fatigue Behaviour of Type 304 Stainless Steel - Grain Size, Prior Cold-Work and Thermal Ageing Effects" - Ph. D.Thesis, Madras University, Jan. 1989.
19. K. Bhanu Sankara Rao, H. Schiffers, H. Schuster and H. Nickel, *Metall, Trans. A.*, 19A (1988), 369.
20. K. Bhanu Sankara Rao, M. Valsan, R. Sandhya, S.L. Mannan and P. Rodriguez, *High Temperature Materials and Processes.*, 7 (1986), 117.
21. K. Bhanu Sankara Rao, H. Schiffers and H. Schuster, In *High Temperature Alloys Their Exploitable Potential*, (eds.) J.B. Marriot, M. Merz, J. Nihoul and J. Wards, Elsevier Applied Science, LONDON, (1987), pp.411-422.
22. M.Valsan, K. Bhanu Sankara Rao and S.L. Mannan, *Trans. IIM*, 42 (SUPPLEMENT) 1969, s203.
23. A.W. Sleeswyk, *Acta Metall.*, 13 (1965), 331.
24. R.E.Read-Hill, *Rev. High. Tem. Mater.*, 2 (1974), 214.
25. S.L. Mannan, K.G. Samuel and P. Rodriguez, *Proc. 6th Intl. Conf., "Strength of Metals and Alloys"*, Melbourne, 1982, (Ed.) R.C. Gifkins, Pergamon Press, New York, 2 (1982), pp. 634-642.
26. R.T. King, J.O. Stiegler and G.M. Goodwin, *Welding Journal, Research Supplement.*, 54 (1974).
27. C.E. Feltner and P. Beardmore, *ASTM STP.*, 467 (1970), 77.
28. A.M. Sherman, *Metall, Trans, A.*, 6A (1975), 1035.
29. W.J. Plumbridge and D.A. Ryder, *Metallurgical Reviews.*, 14 (1969), 119.
30. J.D. Morrow, *ASTM STP.*, 378 (1968), 45.
31. J.O. Nilsson and T. Thorvaldson, *Fat. and Fract. Engng. Mater. and Struct.*, 8 (1985), 373.
32. R.E. Sanders and E.A. Starke, Jr., *Mat. Sci. Engng.*, 28 (1977), 53.
33. K. Hornbogen and K.H. Zum Gahr, *Acta Metall.*, 24 (1976), 581.
34. P.G. Forrest and A.E.L. Tata, *J. Inst. Met.*, 93 (1965), 438.
35. R.M. Pelloux, In *Ultrafine-Grain Metals*, Syracuse University Press, Syracuse, New York (1970), pp.231-243.
36. D.Eylon and P.J. Bania. *Metall, Trans A.*, 9A (1978), 1273.
37. D. Sidey and L.F. Coffin, Jr., *ASTM STP.*, 675 (1979), 528.
38. B.K. Min and R. Raj. *ASTM STP.*, 675 (1979), 569.
39. S.S. Manson, *ASTM STP.*, 520 (1973), 744.
40. C.J. McMahan and L.F. Coffin, Jr., *Metall, Trans.*, 1 (1970), 3443.
41. L.A. James, *Welding Journal (Research Supplement)*, 52 (1973), 173s.
42. R.Shehinian, H.H. Smith and J.R. Hawthorne, *Welding Journal (Research Supplement)*, 51 (1972), 527s.
43. D.T. Raske and C.F. Cheng, *Nuclear Technology*, 34 (1977), 101.



Fight against industrial wear problems...

VAUTID technology made available by Kilburn Engineering Ltd.

VAUTID has more than forty years of experience in developing and producing innovative materials to solve your wear problems.

Hammer Mills, Grinder Rolls, Chutes, Screens, Excavator Buckets, Screw Conveyors, Furnace Top Bells, Liner Plates, Valves, Pumps, Crushers, Ventilators... are subjected to severe wear problems.

KILBURN ENGINEERING LTD offers innovative solutions to your wear problems, reduce your costs and fetch you profits!

For further details please contact Business Development Manager



Kilburn Engineering Limited

Subash Nagar, Bhandup, BOMBAY-400 078.
Tel.: 5613101-02-03. Cable: KILINDRY Telex: 011-71997
Fax: (022) 561-8436

